SUPPLEMENT– ALL-SKY, ALL-FREQUENCY DIRECTIONAL SEARCH FOR PERSISTENT GRAVITATIONAL WAVES FROM ADVANCED LIGO'S AND ADVANCED VIRGO'S FIRST THREE OBSERVING RUNS

In this supplement, we show the ASAF search results for the individual baselines (HL, HV, and LV) from different observation runs. As we mention in the letter, the inclusion of different baselines and observing runs improves the 95% upper limit placed on the strain. By comparing the median values of the upper limit for O1 (HL) and O3 (HLV) data set, as shown in Table. I, one sees an improvement by a factor of ~ 2.8. Since the LIGO detectors are more sensitive than the Virgo detectors, the upper limits from the entire O3 data set is dominated by the Hanford-Livingston baseline. However, the inclusion of Virgo detectors (HV and LV baselines) reduces the fraction of completely notched frequencies in the whole analysis.

In Fig. 1 we provide the BBR SNR sky maps obtained from the O2 HL dataset including the hardware injections. These plots show that the ASAF search is capable of identifying the narrowband signals in comparison to the BBR search since we do not find any evidence of an outlier with the latter search.

In Fig. 2 we provide the distribution of SNR at each frequency and pixel on the sky for O3 data set from the individual baselines. Here one can clearly see that for HL, HV, and LV (from left to right) the SNR distribution follows the noise background and are consistent with Gaussian noise within 2σ error bars. In Fig. 3 we show the 95% confidence Bayesian upper limit on the strain amplitude h for all-sky directions and all-frequency bins using O3 data from all the three baselines (HL, HV, LV from left to right). The standard deviation computed for O1+O2 data set from HL baseline, O3 data set from combined HLV baseline, and O1+O2+O3 data set from HLV baselines are shown in Fig. 4 from left to right. Note that some of the frequencies are notched in all the baselines or observational runs, which appear as blank horizontal bands, while some are notched in specific baseline or observational runs, which appear as discrete bands along with patterns describing the upper limits determined by the other baselines or observational runs. In Fig. 5 we show example plots for the standard deviation computed for O1+O2+O3 data set for three frequencies 23.0625 Hz, 423.0635 Hz, 1223.0625 Hz (from left to right).

95% UL on Strain $h(f, \hat{\mathbf{n}})$	
Baseline / Run	UL range (median) ($\times 10^{-24}$)
O1 - HL	0.093 - 8.5 (0.39)
O2 - HL	0.059 - 4.1 (0.26)
O3 - HL	0.035 - 2.6 (0.14)
O3 - HV	0.068 - 11 (0.47)
O3 - LV	0.074 - 9.6 (0.38)
O1 + O2 + O3 (HLV)	0.030 - 9.6 (0.14)

TABLE I. Strain upper limits computed using the ASAF estimator from the all available data set. The upper limits improve with the inclusion of multiple detectors. When a frequency bin is notched in one baseline, the upper limit is set by the other four data set and baseline combination; hence it becomes weaker (for example, the maximum of the upper limit in O1+O2+O3 (HLV), that corresponds to a unnotched line 20.0625 Hz in the LV baseline only, is higher than the maximum upper limit in HL. However all baselines/runs contribute to the minimum of upper limit which corresponds to frequency 207.6875 Hz).

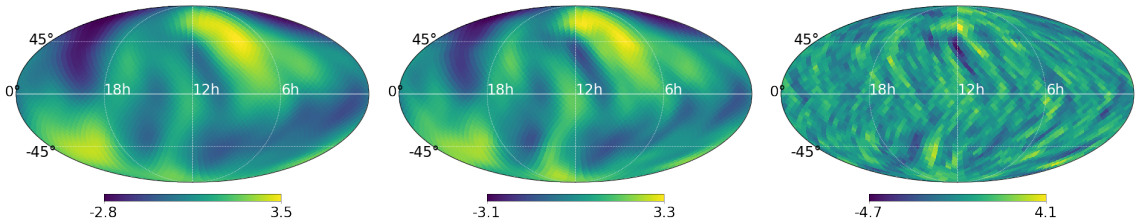

FIG. 1. BBR SNR sky map obtained from the O2 data set (including hardware injections) for the three spectral indices $\alpha = 0, 2/3, 3$ from left to right respectively. In contrast to the ASAF analysis, the obtained maximum SNR in any of these cases did not cross the 5% p-value threshold of 3.6, 4.0 and 4.4 respectively computed from the broadband analysis of timeshifted data. These sky maps are represented as a color bar plot on a Mollweide projection of the sky in ecliptic coordinates. All these sky maps are produced at a `HEALPix` resolution of $N_{\rm side} = 16$.

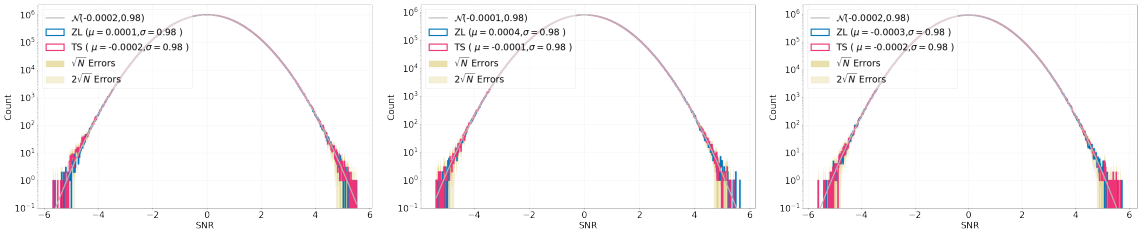

FIG. 2. Distributions of SNR from the individual baselines (HL, HV, LV from left to right) O3 data set are shown. Histogram of SNR from the time-shifted analysis is in red and from zero-lag analysis is in blue. Both the physical and unphysical time-shifted data set are consistent with Gaussian noise (grey histogram) within the 2σ error bars.

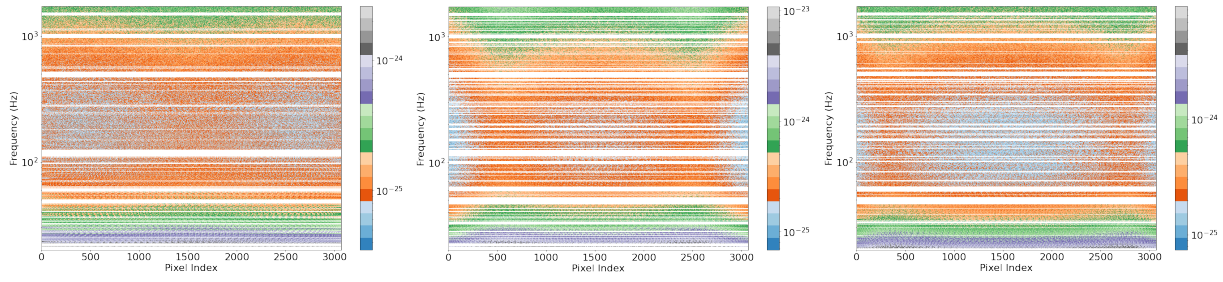

FIG. 3. The Bayesian upper limit on the strain amplitude with 95% confidence using O3 ASAF estimators for the individual baselines HL, HV, LV (from left to right).

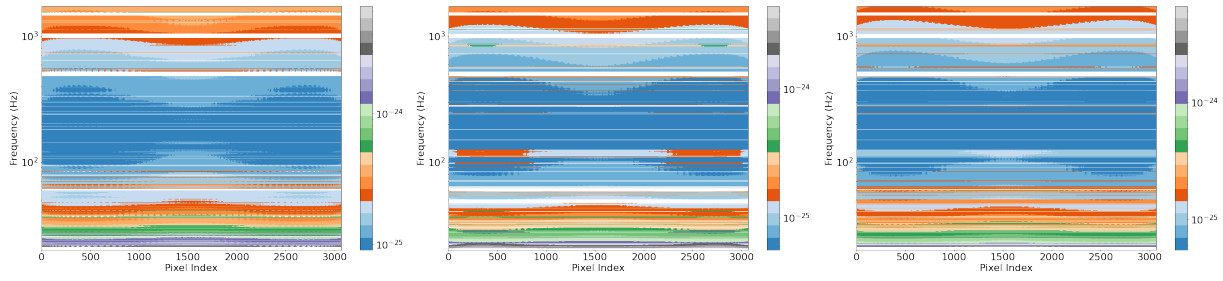

FIG. 4. Standard deviation from O1+O2(HL), O3 (HLV) and O1+O2+O3 (HLV) for all frequency and pixel. The color bar here denotes the range of standard deviation values.

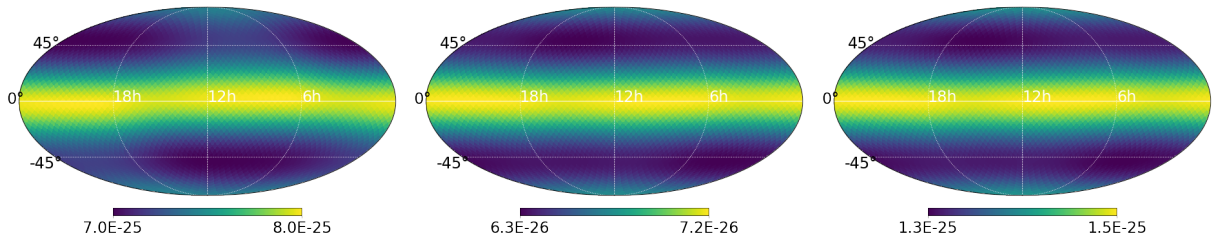

FIG. 5. Standard deviation sky map obtained from the O1+O2+O3 data set for three frequencies [23.0625, 423.0635, 1223.0625] Hz. These sky maps are represented as a color bar plot on a Mollweide projection of the sky in ecliptic coordinates. All these sky maps are produced at a `HEALPix` resolution of $N_{\rm side} = 16$.